

This is a repository copy of *No Detectable Effect on Visual Responses Using Functional MRI in a Rodent Model of  $\alpha$ -Synuclein Expression*.

White Rose Research Online URL for this paper:

<https://eprints.whiterose.ac.uk/174627/>

Version: Accepted Version

---

**Article:**

Østergaard, Freja Gam, Skoven, Christian Stald, Wade, Alex R orcid.org/0000-0003-4871-2747 et al. (4 more authors) (2021) No Detectable Effect on Visual Responses Using Functional MRI in a Rodent Model of  $\alpha$ -Synuclein Expression. *eNeuro*. ISSN 2373-2822

<https://doi.org/10.1523/ENEURO.0516-20.2021>

---

**Reuse**

Items deposited in White Rose Research Online are protected by copyright, with all rights reserved unless indicated otherwise. They may be downloaded and/or printed for private study, or other acts as permitted by national copyright laws. The publisher or other rights holders may allow further reproduction and re-use of the full text version. This is indicated by the licence information on the White Rose Research Online record for the item.

**Takedown**

If you consider content in White Rose Research Online to be in breach of UK law, please notify us by emailing [eprints@whiterose.ac.uk](mailto:eprints@whiterose.ac.uk) including the URL of the record and the reason for the withdrawal request.

---

*Research Article: Negative Results | Disorders of the Nervous System*

## No detectable effect on visual responses using functional MRI in a rodent model of $\alpha$ -synuclein expression

<https://doi.org/10.1523/ENEURO.0516-20.2021>

**Cite as:** eNeuro 2021; 10.1523/ENEURO.0516-20.2021

Received: 30 November 2020

Revised: 23 April 2021

Accepted: 30 April 2021

---

*This Early Release article has been peer-reviewed and accepted, but has not been through the composition and copyediting processes. The final version may differ slightly in style or formatting and will contain links to any extended data.*

**Alerts:** Sign up at [www.eneuro.org/alerts](http://www.eneuro.org/alerts) to receive customized email alerts when the fully formatted version of this article is published.

Copyright © 2021 Østergaard et al.

This is an open-access article distributed under the terms of the Creative Commons Attribution 4.0 International license, which permits unrestricted use, distribution and reproduction in any medium provided that the original work is properly attributed.

1 **Title:** No detectable effect on visual responses using functional MRI in a rodent model of  $\alpha$ -synuclein  
2 expression

3 **Abbreviated title:** fMRI of  $\alpha$ -synuclein model of Parkinson's Disease

4 Freja Gam Østergaard<sup>1</sup>, Christian Stald Skoven<sup>3</sup>, Alex R. Wade<sup>2</sup>, Hartwig R. Siebner<sup>3</sup>, Bettina Laursen<sup>1</sup>,  
5 Kenneth Vielsted Christensen<sup>1</sup>, Tim B. Dyrby<sup>3,4</sup>

6 <sup>1</sup> Circuit Biology, H. Lundbeck A/S, Ottiliavej 9. DK-2500 Valby, Denmark.

7 <sup>2</sup> Department of Psychology, The University of York, Heslington, York, YO10 5DD, United Kingdom.

8 <sup>3</sup> Danish Research Centre for Magnetic Resonance, Centre for Functional and Diagnostic Imaging and  
9 Research, Copenhagen University Hospital - Amager and Hvidovre, Copenhagen, Denmark

10 <sup>4</sup> Department of Applied Mathematics and Computer Science, Technical University of Denmark, 2800  
11 Kongens Lyngby, Denmark

12

13 **Author contributions:** KVC and FGØ conceived and designed the experiments, FGØ, CS and TD  
14 performed the experiments, FGØ analysed the data, all authors wrote the manuscript.

15 **Corresponding Author:** Freja Gam Østergaard, f.g.ostergaard@rug.nl

16 **Figures:** 5 figures and 1 table in main article, no extended data

17 **Number of Words in text:** abstract 246 words, introduction 730 words, discussion 1097 words

18 **Funding Sources:** This project has received funding from the European Union's Horizon 2020 research  
19 and innovation programme under the Marie Skłodowska-Curie grant agreement No 641805. HRS holds a  
20 5-year professorship in precision medicine at the Faculty of Health Sciences and Medicine, University of  
21 Copenhagen which is sponsored by the Lundbeck Foundation (Grant Nr. R186-2015-2138).

22 **Conflicts of Interest:** Hartwig R. Siebner has received honoraria as speaker from Sanofi Genzyme,  
23 Denmark and Novartis, Denmark, as consultant from Lundbeck AS, Denmark and Sanofi Genzyme,  
24 Denmark, and as senior editor (NeuroImage) and Editor-in-Chief (Neurimage-Clinical) from Elsevier  
25 Publishers, Amsterdam, The Netherlands. He has received royalties as book editor from Springer  
26 Publishers, Stuttgart, Germany, and Gyldendal, Copenhagen, Denmark.

27 **Acknowledgements:** The authors would like to thank Sascha Gude, Yi He and Milena Kaestner for their  
28 technical assistance.

29

30

## 31 Abstract

32 Parkinson's disease (PD) is a progressive neurodegenerative disease that is typically diagnosed late in its  
33 progression. There is a need for biomarkers suitable for monitoring the disease progression at earlier  
34 stages to guide the development of novel neuroprotective therapies. One potential biomarker,  $\alpha$ -  
35 synuclein, has been found in both the familial cases of PD, as well as the sporadic cases and is  
36 considered a key feature of PD.  $\alpha$ -synuclein is naturally present in the retina, and it has been suggested  
37 that early symptoms of the visual system may be used as a biomarker for PD.

38 Here, we use a viral vector to induce a unilateral expression of human wildtype  $\alpha$ -synuclein in rats as a  
39 mechanistic model of protein aggregation in PD. We employed functional magnetic resonance imaging  
40 (fMRI) to investigate whether adeno-associated virus (AAV) mediated expression of human wildtype  $\alpha$ -  
41 synuclein alter functional activity in the visual system. 16 rats were injected with either AAV- $\alpha$ -synuclein  
42 (n=7) or AAV-null (n=9) in the *substantia nigra pars compacta* of the left hemisphere. The expression of  
43  $\alpha$ -synuclein was validated by a motor assay and post-mortem immunohistochemistry. Five months after  
44 the introduction of the AAV-vector, fMRI showed robust blood oxygen level dependent (BOLD)  
45 responses to light stimulation in the visual systems of both control and AAV- $\alpha$ -synuclein animals.  
46 However, our results demonstrate that the expression of AAV- $\alpha$ -synuclein does not affect functional  
47 activation of the visual system. This negative finding suggests that fMRI-based read-outs of visual  
48 responses may not be a sensitive biomarker for PD.

49

## 50 Significance statement

51 We injected an adeno-associated virus (AAV) vector in rats to induce unilateral expression of human  
52 wildtype  $\alpha$ -synuclein in the substantia nigra, and in the ipsilateral striatum and superior colliculus (SC).  
53 This did not affect functional activation of SC as probed with functional MRI. This negative finding

- 54 discourages the use of functional brain mapping of visually evoked activity as an indicator of regional  
55 expression of human  $\alpha$ -synuclein.

## 56 Introduction

57 Parkinson's disease (PD) is the second most common neurodegenerative disorder (Wirdefeldt et al.,  
58 2011) affecting millions of people worldwide (Thomas and Beal, 2007). Though the disease is primarily  
59 considered to be sporadic, there are familial versions caused by a mutation in a single gene (Klein and  
60 Westenberger, 2012). These heritable forms of PD have led to the discovery of several susceptibility  
61 genes, such as the *SNCA* gene (park1/4) coding for  $\alpha$ -synuclein. Aggregation of  $\alpha$ -synuclein into fibrils  
62 and Lewy bodies is hypothesized to develop long before the diagnostic symptoms of tremor and  
63 postural instability (Noyce et al., 2016). These aggregates have been proposed to give rise to symptoms  
64 early in the course of the disease, consequently, they may potentially serve as biomarkers for the  
65 progression.

66 This study focuses on the visual system as several studies have shown that the visual system is affected  
67 in PD patients (Davidsdottir et al., 2005; Ekker et al., 2017; Satue et al., 2017). Moreover, these changes  
68 have so far failed to provide an unambiguous estimate of disease severity (Ridder et al., 2017). This is  
69 likely due to PD being diagnosed at a very late stage of disease progression, where patients are prone to  
70 suffer from a wide range of visual changes related to normal aging (Ekker et al., 2017). However,  
71 evidence of PD-related changes in vision was provided by *post mortem* studies showing  $\alpha$ -synuclein  
72 aggregation in the retinae of PD patients (Bodis-Wollner et al., 2014). This finding lead to the hypothesis  
73 that  $\alpha$ -synuclein aggregation may cause changes in visual responses measured in patients with PD.

74 A rodent model of  $\alpha$ -synuclein expression in the *substantia nigra pars compacta* (SNc), mediated by the  
75 adeno-associated virus (AAV) has shown to decrease the number of spines of the dopaminergic cells,  
76 which in turn have shown to influence the neuronal firing pattern in the *striatum* (Andersen et al., 2018).  
77 In addition to the striatum, the SNc also projects to the *superior colliculus* (SC) which is the primary  
78 region for visual processing in rats (Sefton et al., 2014). Further it was shown by Østergaard and  
79 colleagues that this model also exhibits changes in the latency of the visual evoked potential (VEP)

80 measured in the SC (Østergaard et al., 2020). The neuronal firing pattern was measured invasively using  
81 electrophysiology making it infeasible to apply in humans. Hence, a non-invasive technique is desirable.  
82 Magnetic resonance imaging (MRI) is a non-invasive bioimaging modality, which have been used to  
83 investigate regional changes in brain structure of PD patients (Lehéricy et al., 2014). Most MRI-based  
84 studies of PD patients have focused on changes in brain structure (Niethammer et al., 2012; Weil et al.,  
85 2016). Functional MRI (fMRI) measures the local changes in blood oxygenation related to neuronal  
86 activity and has been applied in PD patients to study changes in neuronal function. One of these studies  
87 have shown changes in the iron load of cortex and SNc in PD patients (Pyatigorskaya et al., 2014). fMRI  
88 may also detect neuronal changes in the dopamine release after a pharmacological challenge in the  
89 rodent PD model (Kuebler et al., 2017) also used by Andersen and colleagues (Andersen et al., 2018).  
90 This model mimics the mechanistic changes of expressing human wildtype  $\alpha$ -synuclein in neurons of the  
91 *substantia nigra* (Decressac et al., 2012).

92 The aim of this study was to use blood-oxygenation level dependent (BOLD) fMRI with a visual flickering  
93 full-field illumination stimulation to examine potential functional consequences of expressing human  
94 wildtype  $\alpha$ -synuclein in the rodent. Adeno-associated virus (AAV) carrying DNA encoding human  
95 wildtype  $\alpha$ -synuclein (*hSNCA*) was unilaterally injected in SNc in rats with the aim of exogenously  
96 expressing the human  $\alpha$ -synuclein protein and was thereby expected to cause an asymmetry of the  
97 BOLD response. In 2013, Bailey et al. described how the cortex responds differently to frequencies  
98 above and below a presentation rate of 10 Hz, therefore we have chosen to use presentation rates of  
99 1Hz and 14 Hz. The response to one frequency could be more sensitive to changes introduced by  
100 expressing human  $\alpha$ -synuclein compared to the response to the other frequency, as responses to these  
101 two frequencies may be governed by different mechanisms (Bailey et al., 2013). We use the regions of  
102 interest (ROIs) of the rodent visual system and then compared them to the olfactory bulb (OB). The OB  
103 is used as a control region, as this region is easy to define and neutral with regards to visual stimuli.

104

105 

## Methods

106 

### Subjects

107 All animal experiments were carried out in accordance with the European Communities Council  
108 Directive (86/609/EEC), and in accordance with Danish law on care of laboratory animals. The protocols  
109 were approved by the Danish Animal Experiments Inspectorate (Forsøgsdyrstilsynet) prior to the  
110 initiation of the study.

111 20 female Sprague-Dawley™ (SD) rats (Taconic, Denmark) weighing ~225g (corresponding to ten weeks  
112 of age) upon arrival were included in the study. The rats underwent surgery and cylinder test at one test  
113 site and were transported to another for MRI scanning. The animals acclimatized to the new housing  
114 facility for at least two weeks before imaging. The home cage environment including light cycle, cages  
115 and enrichment was similar at the two housing facilities. Both had a 12h:12h light:dark cycle (lights on at  
116 06:00hrs). The cages were enriched with nesting material and a red plastic shelter. Access to food  
117 (chow) and water was *ad libitum*.

118 

### Surgery

119 Prior to surgery, each rat was anesthetized using subcutaneous (SC) injections of Hypnorm® (Lundbeck,  
120 Valby, Denmark), midazolam 5 mg/ml (B. Braun, Germany), and saline in a 2:1:1 ratio yielding an  
121 injection volume of 1.7 ml/kg. The rat was placed in a stereotaxic frame and 0.1 ml Marcain (2.5mg/ml  
122 bupivacaine, AstraZeneca, Denmark) was administered locally and subcutaneously (SC) prior to incision.  
123 A small craniotomy ( $\varnothing=1\text{mm}$ ) was made over the *substantia nigra pars compacta* (SNc) of the left  
124 hemisphere (AP: -5.5mm; ML: +2.0mm; DV: -7.2mm relative to Bregma (Paxinos and Watson, 1998) to  
125 allow for injection of 3  $\mu\text{l}$  adeno-associated virus (AAV) 2/5 ( $3 \times 10^{10}$  GC/ml) (Vector biolabs, US), carrying  
126 human wildtype  $\alpha$ -synuclein (*hSNCA*) using methodology as described by Andersen (Andersen et al.,



127 2018). Half of the animals acted as controls by having the empty viral vector injected. The animals were  
128 post-operatively treated with buprenorphine 0.05 mg/kg every 8<sup>th</sup> hour for four days. The rats were  
129 single-housed after the surgery.

### 130 *Cylinder test*

131 To validate the expression of human wildtype  $\alpha$ -synuclein in the basal ganglia, the rats were tested for  
132 motor asymmetry ten weeks after surgery. The animals were recorded with a video camera for five  
133 minutes, while they were freely moving in a Plexiglass cylinder. Paw touches on the side of the cylinder  
134 were counted offline and blinded to the group. The ratio of touches of contralateral paw to total  
135 touches was computed. Animals with an expression of human  $\alpha$ -synuclein were hypothesized to use the  
136 contralateral paw less than the control animals.

### 137 *Magnetic Resonance Imaging*

#### 138 *Preparation for functional MRI*

139 Five months after the viral injection, the rats were anesthetized and scanned in a 7T Bruker Biospec  
140 (Bruker BioSpec 70/20 USR) MRI scanner with an 80 mm radio frequency (RF) transmit quadrature coil  
141 and a 20 mm surface receive coil. The surface receive coil was fixed on top of the head using masking  
142 tape. The position of the surface ensured good signal coverage of the whole brain having the largest  
143 signal sensitivity in the regions of interest: the superior colliculus and visual cortex. Sticky tack (Bantex,  
144 South Africa) was placed in the ears of the rats to reduce harmful effects of MR scanner noise during  
145 scanning. The animals were scanned at the same time of day, on separate days, to minimize variation  
146 caused by the circadian rhythm.

#### 147 *Anaesthesia during scan session*

148 To reduce the unwanted effect of isoflurane on the BOLD signal, we used a combination of low dose  
149 isoflurane and dexmedetomidine (Dexdormitor<sup>®</sup>, Orion Pharma, Finland). Anaesthesia was induced with

150 isoflurane at 5 % and adjusted to 2.5 % while placing a tail-vein catheter. Subsequently,  
151 dexmedetomidine was infused at 0.05 mg/kg/hr (Pawela et al., 2009). When the heart rate decreased to  
152 about 200 bpm, isoflurane was adjusted to 0.5 % (in 1 L of oxygen:medical air, 8:2). The animals  
153 breathed spontaneously, and the respiration rate of the animals was continuously monitored by a  
154 respiration sensor pad (SA Instruments; NY, USA). Blood oxygen saturation and heart rate was  
155 monitored transcutaneously using pulse oximetry (Nonin, MN, USA). The core temperature of the  
156 animals was monitored with a rectal probe and used as feedback to maintain a constant temperature of  
157 37 °C using heated air (SA Instruments; NY, USA). After one hour of infusion, the infusion rate of  
158 dexmedetomidine was increased to 0.1 mg/kg/hr. This concentration is lower than what most literature  
159 recommend (Pawela et al., 2009) because the vasoconstrictive effects of dexmedetomidine made  
160 measuring SpO2 challenging, and this lower concentration turned out to be sufficient.

#### 161 MRI protocols

162 Since the structural T1 weighted is not affected by anaesthesia it was acquired before the fMRI. Before  
163 acquiring the actual fMRI, online fMRI correlation analysis was applied at regular time intervals using a  
164 visual stimulus paradigm. Online fMRI correlation analysis used the Analysis of Functional NeuroImages  
165 (AFNI) software integrated with the fMRI sequence (Cox, 1996). The online fMRI analysis was used to  
166 determine when the impact of isoflurane on the neuronal response and BOLD signal was diminished, i.e.,  
167 washed out. Typically, robust regional BOLD responses were obtained after 180 min.

168 Structural MRI to be aligned with fMRI included a whole brain 3D T1-weighted fast low angle shot  
169 (FLASH) MRI (Repetition time (TR)=1500 ms, Echo time (TE)=8 ms, Inversion time (IR)=103338.0 ms,  
170 isotropic 0.2 mm<sup>3</sup> voxels field of view of 175x80x175 mm<sup>3</sup>, matrix size=35x16x35).

171 The echo-planar image (EPI) MRI had an in-plane voxel size of 0.313 x 0.313 mm with slice thickness of  
172 0.500 mm, TR=1500 ms, and TE=8.35 ms, slice gap=0. The Ernst flip angle was determined to 64°, based

173 on T1 relaxation measurement of cortical grey matter obtained from a separate session (data not  
174 shown). 42 coronal slices covered the range from the caudal part of the olfactory bulb to the caudal part  
175 of the cerebellum.

#### 176 Visual stimulation paradigm for fMRI

177 Visual stimulation was provided by five optical fibres (diameter of 1.5 mm) of “warm white” light  
178 provided by a light emitting diode (LED) source placed outside the scanner. The optical fibres were  
179 placed in front of the animal head as an array. The light intensity during the stimulation was kept at 20 lx,  
180 measured at the level of the eyes using a LED luxmeter (Extech, MA, US).

181 The stimulation paradigm used a block design that was generated by a micro1401 data acquisition unit  
182 (Cambridge Electronic Design Ltd., UK) controlled from Spike2 ver. 7.20 synchronized to TTL triggers  
183 from the scanner. The block design included six task blocks per trial repeated five times, where each task  
184 block lasted for 21 s, equivalent to 14 TRs. Each task block consisted of either 1 Hz or 14 Hz light flicker.  
185 These two frequencies were chosen as one should be just above 10 Hz while the other should be well  
186 below, as 10 Hz is considered to be the threshold for saturation of the visual cortex (Van Camp et al.,  
187 2006). Between task blocks there were a pause of 14 TRs (21s). The visual stimulation paradigm was  
188 repeated five times at each stimulation frequency yielding a total scan time of approximately four hours.

#### 189 fMRI pre-processing

190 MRI data were analysed using the FMRIB software library (FSL) (Woolrich et al., 2009). To make a  
191 standard brain template, the EPIs were aligned within subject using FMRIB’s linear image registration  
192 tool (FLIRT) and then averaged across animals to construct a standard brain template. This template was  
193 used for registration of the data for later analysis.

194 Visual inspection caused exclusion of four rats, as these could not be aligned to the standard template  
195 leaving 16 to be analysed; nine controls and seven AAV- $\alpha$ -synuclein animals.

## 196 Statistical analysis

197 Functional MRI data were analysed using a three-level statistical analysis pipeline implemented in the  
198 FSL expert analysis tool (FEAT). In the first level, the time course of each voxel was fitted with a general  
199 linear model (GLM) to produce a statistical map of the z-scores of the correlation for each voxel within  
200 each of the scans. Each voxel was corrected for family-wise error with a p-threshold of  $p < 0.05$ . Spatial  
201 smoothing was then applied using a Gaussian kernel with full width half maximum of 0.5 mm. In the  
202 second level, the z-statistical maps were averaged for each stimulation frequency within each subject  
203 yielding two averaged z-statistical maps per animal. Each voxel within the averaged statistical map was  
204 corrected for family-wise error with a p-threshold of  $p = 0.05$ . At the third and final level, the averaged  
205 statistical maps were averaged within the two groups for each of the two stimulation frequencies. The  
206 group statistical maps were compared using an unpaired comparison of the z-statistical maps between  
207 the two groups within each frequency paradigm. For visualization, the statistical maps were aligned to  
208 the standard brain template (described above) and then superimposed on the high-resolution structural  
209 MRI scan.

210 Structural regions of interest (ROIs) of the superior colliculus and visual cortex were defined manually  
211 based on rat brain atlases (Kjonigsen et al., 2015; Papp et al., 2014; Sergejeva et al., 2015). The  
212 olfactory bulb (OB) was used as a control ROI. For each group there were ROIs for OB, right SC, left SC,  
213 right VC and left VC. The percent change of the BOLD within the ROIs were extracted from the z-  
214 statistical map of each rat using FEAT query. Further, estimation statistics were carried out using the  
215 website <https://www.estimationstats.com/#/> which is based on the methods described in (Ho et al.,  
216 2019). Here the data were compared with the common control method within each stimulus paradigm,  
217 tested using a two-sided permutation t-test and corrected for multiple comparisons. The resulting effect  
218 sizes and confidence intervals (CI) are listed in table 1.

219

220 **Immunohistochemistry**

221 At the end of the scan session, the animal was given a bolus 3 ml/kg of Hypnorm® and midazolam was  
222 administered SC. The animals were perfusion fixated with intracardial potassium phosphate-buffered  
223 saline (KPBS) for three minutes, followed by 4% paraformaldehyde (PFA) premade with methanol. After  
224 10-15 minutes, the rat was decapitated, and the brain extracted. The brain was immersed in 4% PFA for  
225 2 hours, then in phosphate buffer (PBS) with <1% PFA for 24 hours, and finally in KPBS.

226 Brains were fixed in 30% sucrose for 72 hours before slicing. Once fixed, they were dried and frozen with  
227 dry ice and placed in a freezing microtome (Leica CM3050S) for 30 min. 40 µm thick coronal slices were  
228 cut and stored in KPBS. All slices were stained within five days.

229 Brain sections were stained to validate the expression pattern of the human wild type SNCA protein.  
230 Before staining, the tissue was quenched with hydrogen peroxide 3 % to remove any traces of blood.  
231 The slices were washed and incubated overnight with 4B12 (Thermo Scientific, US) for human α-  
232 synuclein as the primary antibody (concentration 1:1000). Subsequently, the slices were washed and  
233 incubated with biotin conjugated anti-mouse secondary antibody (Jackson ImmunoResearch  
234 Laboratories, MA, US) and exposed using a 3,3'-diaminobenzidine (DAB) reaction for approx. 20 minutes.  
235 The stained slices were placed on gelatine covered glass slides, and visually examined using a light  
236 microscope (Axio scope.A1, Carl Zeiss Microimaging, Germany).

237

## 238 Results

### 239 Motor assessment of $\alpha$ -synuclein expression

240 To validate the expression and impact of human  $\alpha$ -synuclein in the rat basal ganglia,  $\alpha$ -synuclein and  
241 control animals were tested for motor asymmetry in the cylinder test (Andersen et al., 2018). Figure 1A  
242 shows the change in the use of the forepaw contralateral to the injection site. Control animals used both  
243 paws equally (ratio of 0.5) while  $\alpha$ -synuclein animals had a significantly different mean ratio of  
244 affected/total touches ratio of 0.35 ( $t(14)=2.8$ ,  $p=0.01$ ). The cylinder test confirmed that the function of  
245 the striatum was unilaterally affected in the animals that received the AAV-*hSNCA*-injection, as expected  
246 with successful injection of viral particles carrying the *hSNCA*-expressing vector.

247

### 248 Validation of expression of human $\alpha$ -synuclein

249 Immunohistochemical evaluation carried out after fMRI, showed immunoreactivity towards human  $\alpha$ -  
250 synuclein in the SNc (Figure 1 E-F), in areas surrounding the SNc, and in the striatum ipsilateral (Figure B-  
251 C) to the injection site. Interestingly, small inclusions of immunoreactivity were observed in the optic  
252 layer of the ipsilateral superior colliculus (Figure 1G). Minor immunoreactivity was observed along the  
253 edges of the tissue (Figure 1 C-D) which were not specific to the injected hemisphere thus considered as  
254 unspecific immunoreactivity. Confirmation of  $\alpha$ -synuclein in areas ipsilateral to the injected hemisphere  
255 supports the observations from the cylinder test.

256

### 257 fMRI of the visual system

258 The z-statistical maps of the two groups are shown in Figure 2 registered to a high-resolution anatomical  
259 scan. Overall, there were detectable responses in both the SC and the VC during light stimulation in both

260 groups of rats. A modest activation of cerebellar flocculus complex was also observed. This is in line with  
261 previous studies where visual stimulation has been applied (Van Camp et al., 2006). Additionally, there  
262 was a response in the lateral geniculate nucleus (LGN), as expected (Bailey et al., 2013).

263 The BOLD changes from each of the ROIs are visualized as points in the top panels of Figure 3 and 4.  
264 Figure 3 shows the responses to light flashing at 1 Hz. Estimation statistics comparing each ROI to the OB  
265 revealed a significant response in both the VC and SC to the light flashing at 1 Hz (Figure 3). Table 1 lists  
266 the full results with effects sizes and confidence intervals (CI). Figure 4 shows the responses to 14 Hz  
267 flashing light. There was a statistically significant response to the light stimulation in the SC.  
268 Furthermore, a significant difference was shown for VC ipsilateral to the injection of  $\alpha$ -synuclein in the  
269 14 Hz condition, with a magnitude of -0.414 (CI[-0.714,-0.182],  $p=0.0012$ ). However, there was also a  
270 difference in the control with an effect size of -0.424 (CI[-0.785,-0.0208], $p=0.0496$ ) (Figure 4). Taken  
271 together this suggests that the effect was not induced by the expression of  $\alpha$ -synuclein. Regardless, this  
272 potential asymmetry was explored by comparing the VC within animals with a paired, permutation t-test  
273 (Figure 5). The control group showed an insignificant difference between hemispheres measured in the  
274 VC effect size of 0.167 (CI[0.0163,0.324],  $p=0.0932$ ). Similarly, there was no detectable difference  
275 between hemispheres in the  $\alpha$ -synuclein group effect size -0.156 (CI[-0.268,-0.0296], $p=0.064$ ). In  
276 conclusion, the expression of the  $\alpha$ -synuclein did not induce detectable changes in the BOLD response  
277 within animals.

278

279

## 280 Discussion

281 This study examined whether expression of  $\alpha$ -synuclein in the SNc is associated with abnormal visually  
282 evoked brain activation. Using estimation statistics, we found robust BOLD fMRI responses to the visual  
283 stimulus in the SC in both control rats and  $\alpha$ -synuclein rats. The BOLD response in the VC turned out to  
284 be dependent on the presentation rate of the stimulus. A fully developed expression of  $\alpha$ -synuclein in  
285 the SNc, in the optic layer of SC, and in the striatum did not induce any detectable changes in BOLD fMRI  
286 during visual stimulation. This indicates that the level of neuronal activity measured during visual  
287 stimulation was not altered by expression of  $\alpha$ -synuclein. Alternatively, the scan protocol used for BOLD-  
288 fMRI at 7T was not sensitive enough to detect any subtle differences between groups. However, the  
289 BOLD responses in rat visual system reproduced the frequency-dependence of the rodent visual cortex  
290 that was previously reported (Van Camp et al., 2006). For VC, the visually evoked BOLD responses  
291 tended to decrease at stimulation frequencies above 10Hz, similar to the data shown in another study  
292 (Bailey et al., 2013). The BOLD signal in the SC did not show this frequency-response behaviour.

293 The AAV-model was validated both behaviourally and with immunohistochemistry. Previously,  
294 asymmetry in the cylinder test have been shown to be specific to  $\alpha$ -synuclein expression and is not an  
295 effect of induced protein expression with e.g., green fluorescent protein (Andersen et al., 2018). In the  
296 present study it is shown that there is indeed asymmetry in the use of forepaws as measured in the  
297 cylinder test.

298 After the scan sessions the brains of each of the animals were stained for human wild type  $\alpha$ -synuclein  
299 to validate that the model was developed. Both the cylinder test and the immunohistochemistry  
300 confirmed a successful development of human  $\alpha$ -synuclein expression in the SNc and connected areas  
301 such as the striatum and the SC of the  $\alpha$ -synuclein animals. Furthermore, it showed that human  $\alpha$ -  
302 synuclein was present in the SC ipsilateral to the injection, however, this did not cause a detectable



303 asymmetry in the BOLD-response of the SC upon visual stimulation. Previously, the effect of human  $\alpha$ -  
304 synuclein expression in rats was measured using *in vivo* electrophysiology. Here, subtle changes in the  
305 latency of visual evoked potentials in the SC were shown (Østergaard et al., 2020). The temporal  
306 resolution of fMRI might not be suitable to detect subtle increases in latency. This may explain the lack  
307 of difference between the responses in the two hemispheres in the  $\alpha$ -synuclein animals. There is no  
308 direct correlation between event-related potentials and BOLD-fMRI but the  $\gamma$ -band power (Huettel et al.,  
309 2004) and event-related spectral perturbations (Engell et al., 2012) have been shown to correlate with  
310 the BOLD response. The results in this study supports this discrepancy between the techniques.

311 Interestingly, there was a significant difference in the VC compared to the OB in the 14 Hz stimulation. A  
312 decreased BOLD response was observed in the VC ipsilateral to the injection in the  $\alpha$ -synuclein group  
313 and in the VC contralateral to the injection in the control group compared to the OB. However, this was  
314 not due to asymmetry between the hemispheres in any of the groups, suggesting that the observed  
315 effect was not caused by the expression of  $\alpha$ -synuclein.

316 In this study, the rodent eye is not considered to be implicated. Also, the study by Østergaard et al.  
317 (Østergaard et al., 2020) did not show any statistically significant changes in the visual cortex after  
318 injection of AAV carrying human  $\alpha$ -synuclein. If the rodent eye was functionally impacted, then both the  
319 SC and the VC would also have been affected. The AAV virus was injected in the SNc and the virus  
320 particles tend to spread in the area proximal to the injection site and via direct neuronal projections  
321 (Albert et al., 2019). Furthermore, the SNc is not a retinorecipient region of the rat visual system (Sefton  
322 et al., 2014).

323 The AAV  $\alpha$ -synuclein rat model of PD is not known to cause large anatomical changes in the brain,  
324 however, it does show a loss of dopaminergic cells (Decressac et al., 2012). A study by Kuebler and  
325 colleagues suggests that the change in dopamine can be measured by fMRI/PET using an amphetamine

326 challenge (Kuebler et al., 2017). Generally, the functional consequences of expressing human  $\alpha$ -  
327 synuclein *in vivo* have been shown with other MR-based methods than BOLD-fMRI. A study using  
328 diffusion kurtosis imaging imaged  $\alpha$ -synuclein in transgenic mice (Khairnar et al., 2017). This technique  
329 evaluates structural changes instead of the changes in oxygen metabolism. Another study used MR-  
330 spectroscopy to show that bilaterally overexpressing  $\alpha$ -synuclein in the striatum caused changes in  
331 energy metabolism in rats (Cuellar-Baena et al., 2016). This technique is sensitive to changes in amounts  
332 of metabolites where BOLD detects changes in the oxygen metabolism of larger populations of neurons.

333 In rodent models of Alzheimer's disease, changes have been reported in functional connectivity patterns  
334 at early stages of protein aggregation. This has been observed using resting state fMRI (Grandjean et al.,  
335 2014). It can be speculated that this could be caused by protein aggregation and that the specific  
336 composition of proteins may be less important. Thus, evaluation of the AAV-model using functional  
337 connectivity should be investigated further.

338 In human patients, Zhao et al. have described changes in the BOLD signal of visual areas concerned with  
339 the perception of movement (Zhao et al., 2014). Further studies would be needed to study if motion  
340 perception is also affected in the AAV-model. Here, we studied low-level visual processing but higher  
341 order functions such as motion perception may be more sensitive to the presence of  $\alpha$ -synuclein.  
342 Generally, task-related BOLD fMRI is rarely used to study PD in animals and humans. Often resting state  
343 fMRI and diffusion MRI are applied (Lehericy et al., 2017; Tessitore et al., 2019).

344 The necessity of anaesthesia is a major challenge for fMRI studies in rodents. Anaesthesia generally  
345 works by altering the neuronal activity (Masamoto and Kanno, 2012). Consequently, it will also affect  
346 the BOLD response. Unlike urethane and alpha-chloralose, a mix of isoflurane and dexmedetomidine  
347 may be used in longitudinal studies. The anaesthesia paradigm used in the present study showed  
348 detectable and robust activation of the SC three hours after the induction of anaesthesia. As the

349 functional changes in the SC are believed to be subtle, it cannot be ruled out that the effect of the  
350 anaesthesia may mask potential functional differences.

351 In summary, this study shows that the fully developed expression of  $\alpha$ -synuclein in the SNc along with  
352 the optic layer of SC and the striatum, did not induce any asymmetry detectable using BOLD fMRI during  
353 visual stimulation.

354

355

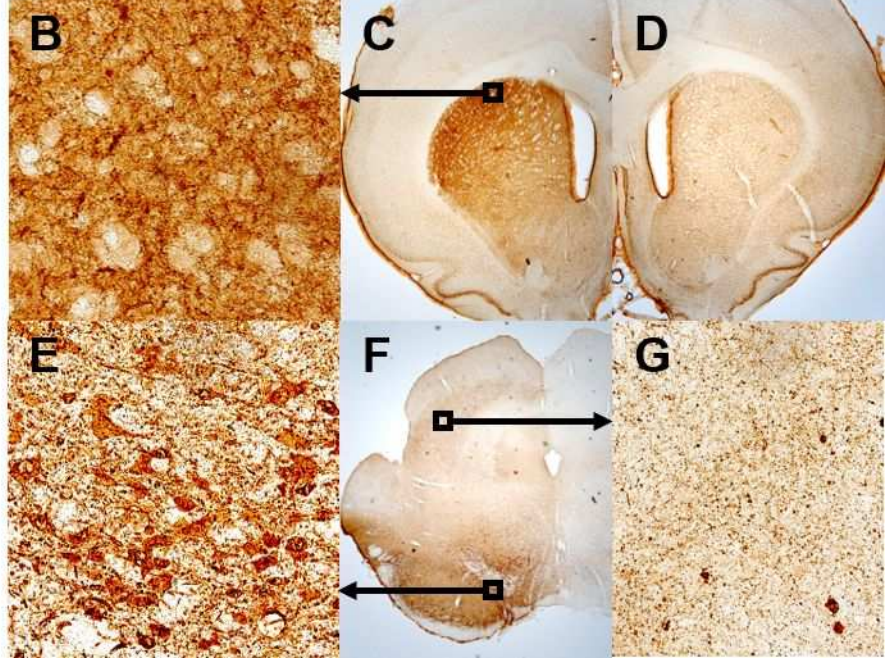
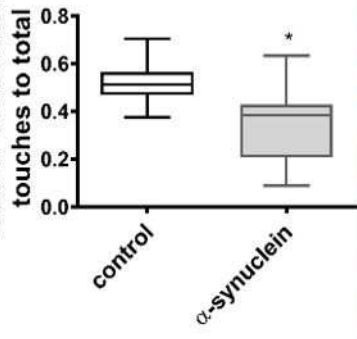
356 **References**

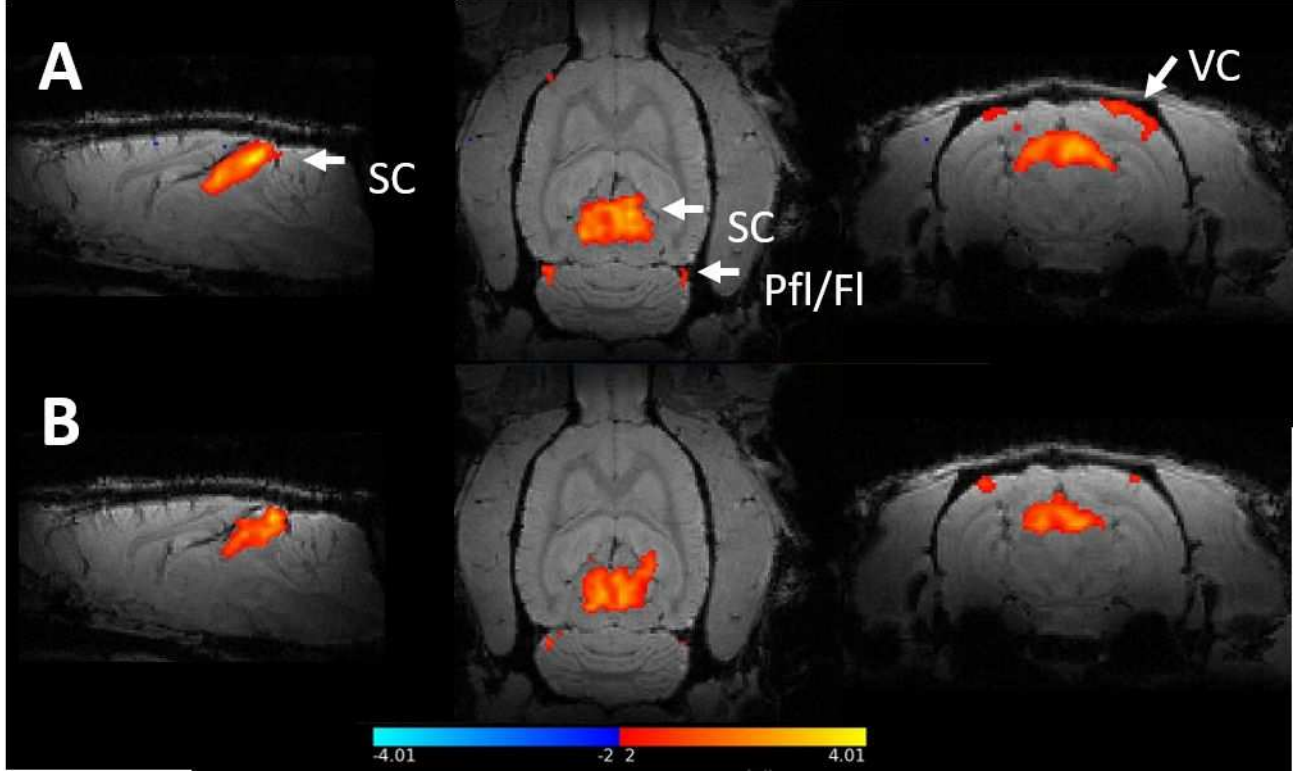
- 357 Albert, K., Voutilainen, M.H., Domanskyi, A., Piepponen, T.P., Ahola, S., Tuominen, R.K., Richie, C.,  
358 Harvey, B.K., Airavaara, M., 2019. Downregulation of tyrosine hydroxylase phenotype after AAV  
359 injection above substantia nigra: Caution in experimental models of Parkinson's disease. *J.*  
360 *Neurosci. Res.* 97, 346–361. <https://doi.org/10.1002/jnr.24363>
- 361 Andersen, M.A., Christensen, K.V., Badolo, L., Smith, G.P., Jeggo, R., Jensen, P.H., Andersen, K.J., Sotty, F.,  
362 2018. Parkinson's disease-like burst firing activity in subthalamic nucleus induced by AAV- $\alpha$ -  
363 synuclein is normalized by LRRK2 modulation. *Neurobiol. Dis.* 116, 13–27.  
364 <https://doi.org/10.1016/j.nbd.2018.04.011>
- 365 Bailey, C.J., Sanganahalli, B.G., Herman, P., Blumenfeld, H., Gjedde, A., Hyder, F., 2013. Analysis of time  
366 and space invariance of BOLD responses in the rat visual system. *Cereb. Cortex* 23, 210–222.  
367 <https://doi.org/10.1093/cercor/bhs008>
- 368 Bodis-Wollner, I., Kozlowski, P.B., Glazman, S., Miri, S., 2014.  $\alpha$ -Synuclein in the Inner Retina in Parkinson  
369 Disease. *Ann. Neurol.* 75, 964–966. <https://doi.org/10.1002/ana.24182>
- 370 Cox, R.W., 1996. AFNI : Software for Analysis and Visualization of Functional Magnetic Resonance  
371 Neuroimages. *Comput. Biomed. Res.* 29, 162–173. <https://doi.org/10.1006/cbmr.1996.0014>
- 372 Cuellar-Baena, S., Landeck, N., Sonnay, S., Buck, K., Mlynarik, V., In 'T Zandt, R., Kirik, D., 2016.  
373 Assessment of brain metabolite correlates of adeno-associated virus-mediated over-expression of  
374 human  $\alpha$ -synuclein in cortical neurons by in vivo  $^1\text{H}$ -MR spectroscopy at 9.4 T. *J. Neurochem.*  
375 137, 806–819. <https://doi.org/10.1111/jnc.13547>
- 376 Davidsdottir, S., Cronin-Golomb, A., Lee, A., 2005. Visual and spatial symptoms in Parkinson's disease.  
377 *Vision Res.* 45, 1285–1296. <https://doi.org/10.1016/j.visres.2004.11.006>
- 378 Decressac, M., Mattsson, B., Lundblad, M., Weikop, P., Björklund, A., 2012. Progressive  
379 neurodegenerative and behavioural changes induced by AAV-mediated overexpression of  $\alpha$ -  
380 synuclein in midbrain dopamine neurons. *Neurobiol. Dis.* 45, 939–953.  
381 <https://doi.org/10.1016/j.nbd.2011.12.013>
- 382 Ekker, M.S., Janssen, S., Seppi, K., Poewe, W., de Vries, N.M., Theelen, T., Nonnekes, J., Bloem, B.R.,  
383 2017. Ocular and visual disorders in Parkinson's disease: Common but frequently overlooked. *Park.*  
384 *Relat. Disord.* 40, 1–10. <https://doi.org/10.1016/j.parkreldis.2017.02.014>
- 385 Engell, A.D., Huettel, S., McCarthy, G., 2012. The fMRI BOLD signal tracks electrophysiological spectral  
386 perturbations, not event-related potentials. *Neuroimage* 59, 2600–2606.  
387 <https://doi.org/10.1016/j.neuroimage.2011.08.079>
- 388 Grandjean, J., Schroeter, A., He, P., Tanadini, M., Krstic, D., Keist, R., Konietzko, U., Klohs, J., Nitsch, R.M.,  
389 Rudin, M., 2014. Early Alterations in Functional Connectivity and White Matter Structure in a  
390 Transgenic Mouse Model of Cerebral Amyloidosis. *J. Neurosci.* 34, 13780–13789.  
391 <https://doi.org/10.1523/jneurosci.4762-13.2014>
- 392 Ho, J., Tumkaya, T., Aryal, S., Choi, H., Claridge-Chang, A., 2019. Moving beyond P values: data analysis  
393 with estimation graphics. *Nat. Methods* 16, 565–566. <https://doi.org/10.1038/s41592-019-0470-3>

- 394 Huettel, S.A., McKeown, M.J., Song, A.W., Hart, S., Spencer, D.D., Allison, T., McCarthy, G., 2004. Linking  
395 Hemodynamic and Electrophysiological Measures of Brain Activity: Evidence from Functional MRI  
396 and Intracranial Field Potentials. *Cereb. Cortex* 14, 165–173.  
397 <https://doi.org/10.1093/cercor/bhg115>
- 398 Khairnar, A., Ruda-Kucerova, J., Szabó, N., Drazanova, E., Arab, A., Hutter-Paier, B., Neddens, J., Latta, P.,  
399 Starcuk, Z., Rektorova, I., 2017. Early and progressive microstructural brain changes in mice  
400 overexpressing human  $\alpha$ -Synuclein detected by diffusion kurtosis imaging. *Brain. Behav. Immun.* 61,  
401 197–208. <https://doi.org/10.1016/j.bbi.2016.11.027>
- 402 Kjonigsen, L.J., Lillehaug, S., Bjaalie, J.G., Witter, M.P., Leergaard, T.B., 2015. Waxholm Space atlas of the  
403 rat brain hippocampal region: Three-dimensional delineations based on magnetic resonance and  
404 diffusion tensor imaging. *Neuroimage* 108, 441–449.  
405 <https://doi.org/10.1016/j.neuroimage.2014.12.080>
- 406 Klein, C., Westenberger, A., 2012. Genetics of Parkinson's Disease. *Cold Spring Harbor Perspect. Med.* 2,  
407 1–15. <https://doi.org/10.1016/j.jconrel.2014.05.021>
- 408 Kuebler, L., Herfert, K., Landeck, N., Maurer, A., Amend, M., Thielcke, A., Buss, S., Marciano, S., Stumm,  
409 R., Wehrl, H.F., Kirik, D., Pichler, B.J., 2017. Quantification of molecular and functional changes in a  
410 rat model of Parkinson's disease using a simultaneous PET/fMRI protocol.
- 411 Lehéricy, S., Bardinnet, E., Poupon, C., Vidailhet, M., François, C., 2014. 7 tesla magnetic resonance  
412 imaging: A closer look at substantia nigra anatomy in Parkinson's disease. *Mov. Disord.* 29, 1574–  
413 1581. <https://doi.org/10.1002/mds.26043>
- 414 Lehericy, S., Vaillancourt, D.E., Seppi, K., Monchi, O., Rektorova, I., Antonini, A., McKeown, M.J., Masellis,  
415 M., Berg, D., Rowe, J.B., Lewis, S.J.G., Williams-Gray, C.H., Tessitore, A., Siebner, H.R., 2017. The  
416 role of high-field magnetic resonance imaging in parkinsonian disorders: Pushing the boundaries  
417 forward. *Mov. Disord.* 32, 510–525. <https://doi.org/10.1002/mds.26968>
- 418 Masamoto, K., Kanno, I., 2012. Anesthesia and the quantitative evaluation of neurovascular coupling. *J.*  
419 *Cereb. Blood Flow Metab.* 32, 1233–1247. <https://doi.org/10.1038/jcbfm.2012.50>
- 420 Niethammer, M., Feigin, A., Eidelberg, D., 2012. Functional neuroimaging in Parkinson's disease. *Cold*  
421 *Spring Harb. Perspect. Med.* 2, 1–21. <https://doi.org/10.1101/cshperspect.a009274>
- 422 Noyce, A.J., Lees, A.J., Schrag, A.-E., 2016. The prediagnostic phase of Parkinson's disease. *J. Neurol.*  
423 *Neurosurg. Psychiatry* 87, 871–878. <https://doi.org/10.1136/jnnp-2015-311890>
- 424 Østergaard, F.G., Himmelberg, M.M., Laursen, B., Siebner, H.R., Wade, A.R., Christensen, K.V., 2020.  
425 Classification of  $\alpha$ -synuclein-induced changes in the AAV  $\alpha$ -synuclein rat model of Parkinson's  
426 disease using electrophysiological measurements of visual processing. *Sci. Rep.* 10, 1–14.  
427 <https://doi.org/10.1038/s41598-020-68808-3>
- 428 Papp, E.A., Leergaard, T.B., Calabrese, E., Johnson, G.A., Bjaalie, J.G., 2014. Waxholm Space atlas of the  
429 Sprague Dawley rat brain. *Neuroimage* 97, 374–386.  
430 <https://doi.org/10.1016/j.neuroimage.2014.04.001>
- 431 Pawela, C.P., Biswal, B.B., Hudetz, A.G., Schulte, M.L., Li, R., Jones, S.R., Cho, Y.R., Matloub, H.S., Hyde,  
432 J.S., 2009. A protocol for use of medetomidine anesthesia in rats for extended studies using task-

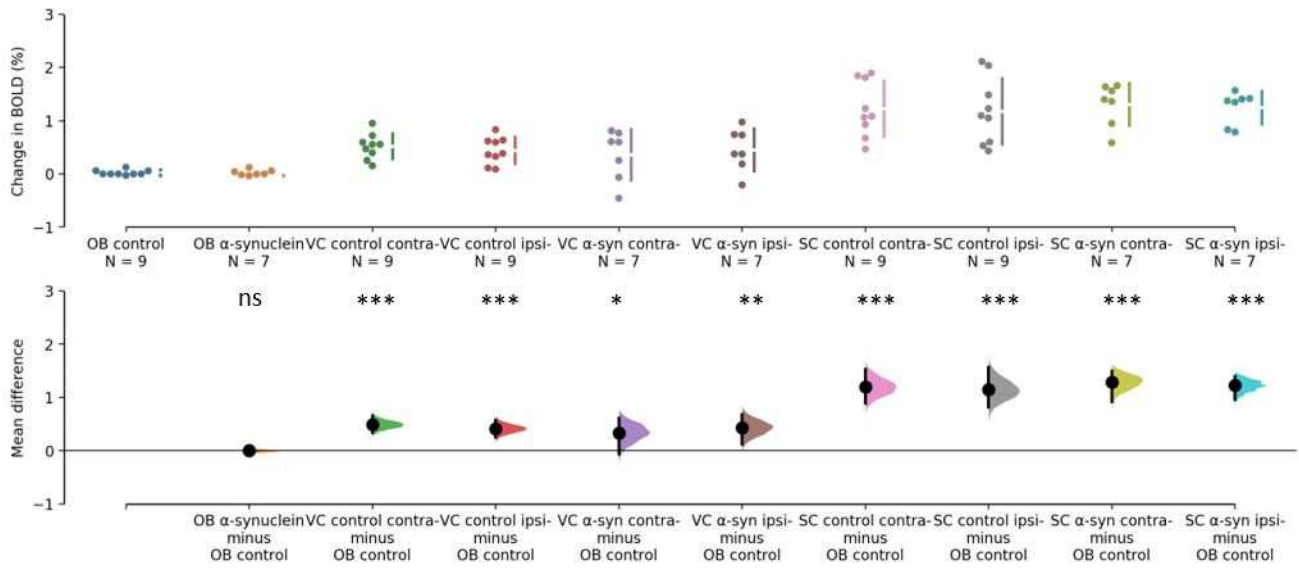
- 433 induced BOLD contrast and resting- state functional connectivity. *Neuroimage* 46, 1137–1147.  
434 <https://doi.org/10.1016/j.neuroimage.2009.03.004>
- 435 Paxinos, G., Watson, C., 1998. *The Rat Brain: in stereotaxic Coordinates*, 4th ed. Academic Press, An  
436 imprint of Elsevier, San Diego, London.
- 437 Pyatigorskaya, N., Gallea, C., Garcia-Lorenzo, D., Vidailhet, M., Lehericy, S., 2014. A review of the use of  
438 magnetic resonance imaging in Parkinson’s disease. *Ther. Adv. Neurol. Disord.* 7, 206–220.  
439 <https://doi.org/10.1177/1756285613511507>
- 440 Ridder, A., Müller, M.L.T.M., Kotagal, V., Frey, K.A., Albin, R.L., Bohnen, N.I., 2017. Impaired contrast  
441 sensitivity is associated with more severe cognitive impairment in Parkinson disease. *Park. Relat.*  
442 *Disord.* 34, 15–19. <https://doi.org/10.1016/j.parkreldis.2016.10.006>
- 443 Satue, M., Rodrigo, M.J., Obis, J., Vilades, E., Gracia, H., Otin, S., Fuertes, M.I., Alarcia, R., Crespo, J.A.,  
444 Polo, V., Larrosa, J.M., Pablo, L.E., Garcia-Martin, E., 2017. Evaluation of progressive visual  
445 dysfunction and retinal degeneration in patients with parkinson’s disease. *Investig. Ophthalmol. Vis.*  
446 *Sci.* 58, 1151–1157. <https://doi.org/10.1167/iovs.16-20460>
- 447 Sefton, A.J., Dreher, B., Harvey, A.R., Martin, P.R., 2014. *Visual System, The Rat Nervous System: Fourth*  
448 *Edition.* <https://doi.org/10.1016/B978-0-12-374245-2.00030-9>
- 449 Sergejevaa, M., Papp, E.A., Bakker, R., Gaudneka, M.A., Okamura-Ohoe, Y., Bolinef, J., Bjaalieb, J.G.,  
450 Andreas, H., 2015. Anatomical landmarks for registration of experimental image data to volumetric  
451 rodent brain atlas templates. *J. Neurosci. Methods* 240, 161–169.  
452 <https://doi.org/10.1016/j.jneumeth.2014.11.005>
- 453 Tessitore, A., Cirillo, M., De Micco, R., 2019. Functional Connectivity Signatures of Parkinson’s Disease. *J.*  
454 *Parkinsons. Dis.* 9, 637–652. <https://doi.org/10.3233/JPD-191592>
- 455 Thomas, B., Beal, M.F., 2007. Parkinson’s disease. *Hum. Mol. Genet.* 16, R183–R194.  
456 [https://doi.org/10.1007/978-1-4939-7880-9\\_5](https://doi.org/10.1007/978-1-4939-7880-9_5)
- 457 Van Camp, N., Verhoye, M., De Zeeuw, C.I., Van der Linden, A., 2006. Light Stimulus Frequency  
458 Dependence of Activity in the Rat Visual System as Studied With High-Resolution BOLD fMRI. *J.*  
459 *Neurophysiol.* 95, 3164–3170. <https://doi.org/10.1152/jn.00400.2005>
- 460 Weil, R.S., Schrag, A.E., Warren, J.D., Crutch, S.J., Lees, A.J., Morris, H.R., 2016. Visual dysfunction in  
461 Parkinson’s disease. *Brain* 139, 2827–2843. <https://doi.org/10.1093/brain/aww175>
- 462 Wirdefeldt, K., Adami, H., Cole, P., Trichopoulos, D., Mandel, J., 2011. Epidemiology and etiology of  
463 Parkinson ’ s disease : a review of the evidence. *Eur. J. Epidemiol.* 26, S1–S58.  
464 <https://doi.org/10.1007/s10654-011-9581-6>
- 465 Woolrich, M.W., Jbabdi, S., Patenaude, B., Chappell, M., Makni, S., Behrens, T., Beckmann, C., Jenkinson,  
466 M., Smith, S.M., 2009. Bayesian analysis of neuroimaging data in FSL. *Neuroimage* 45, S173–S186.  
467 <https://doi.org/10.1016/j.neuroimage.2008.10.055>
- 468 Zhao, Y., Zheng, X., Wang, Q., Xu, J., Xu, X., Zhang, M., 2014. Altered activation in visual cortex: unusual  
469 functional magnetic resonance imaging finding in early Parkinson’s disease. *J. Int. Med. Res.* 42,  
470 503–15. <https://doi.org/10.1177/0300060513507647>

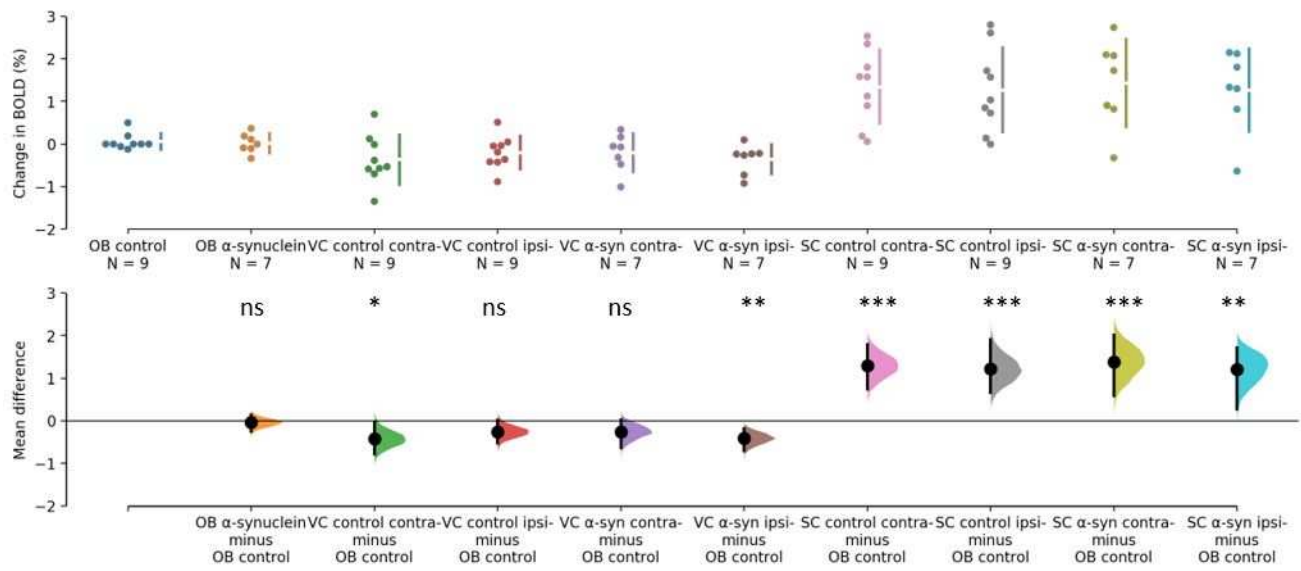
**A**  
ratio of contralateral  
touches to total











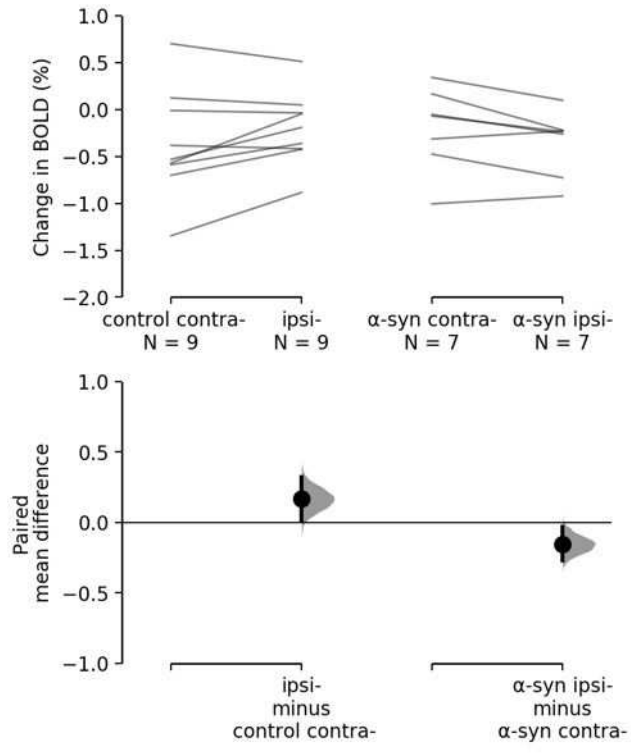


Table 1

Figure	Stimulus	Control ROI	ROI	Effect size	CI (width 95.0 %)		p-value
					Lower bound	Upper bound	
3	1 Hz	OB control	OB $\alpha$ -synuclein	-0.000905	-0.00444	0.0502	0.981
			VC control contra-	0.493	0.344	0.651	0.00022
			VC control ipsi-	0.415	0.255	0.568	0.00099
			VC $\alpha$ -synuclein contra-	0.336	-0.0667	0.609	0.0452
			VC $\alpha$ -synuclein ipsi-	0.429	0.127	0.68	0.0044
			SC control contra-	1.2	0.885	1.52	0.000123
			SC control ipsi-	1.15	0.816	1.57	0.000498
			SC $\alpha$ -synuclein contra-	1.28	0.917	1.5	0.000133
			SC $\alpha$ -synuclein ipsi-	1.22	0.958	1.4	0.000036
4	14 Hz	OB control	OB $\alpha$ -synuclein	-0.038	-0.243	0.14	0.722
			VC control contra-	-0.424	-0.785	-0.0208	0.0496
			VC control ipsi-	-0.257	-0.528	0.0135	0.0926
			VC $\alpha$ -synuclein contra-	-0.258	-0.638	0.0227	0.139
			VC $\alpha$ -synuclein ipsi-	-0.414	-0.714	-0.182	0.0012
			SC control contra-	1.29	0.744	1.8	0.0006
			SC control ipsi-	1.22	0.66	1.9	0.0006
			SC $\alpha$ -synuclein contra-	1.38	0.585	2.01	0.001
			SC $\alpha$ -synuclein ipsi-	1.21	0.273	1.72	0.0026